Nuclear structure studies of ^{24}F

L. Caceres, A. Lepailleur, O. Sorlin, M. Stanoiu, D. Sohler, Zs. Dombradi, S. K. Bogner, B.A. Brown, H. Hergert, J.D. Holt, et al.

Nuclear structure studies of ^{24}F

L. Cáceres,[1] A. Lepailleur,[1] O. Sorlin,[1] M. Stanoiu,[1,2,3] D. Sohler,[4] Zs. Dombrádi,[4] S. K. Bogner,[5] B. A. Brown,[5] H. Hergert,[5] J. D. Holt,[6,7,8,5] A. Schwenk,[7,8] F. Azaiez,[2] B. Bastin,[1] C. Borcea,[3] R. Borcea,[3] C. Bourgeois,[2] Z. Elekes,[5] Zs. Fülöp,[4] S. Grévy,[1,9] L. Gaudefroy,[10] G. F. Grinyer,[1] D. Guillemaud-Mueller,[2] F. Ibrahim,[2] A. Kerek,[11] A. Krasznahorkay,[4] M. Lewitowicz,[1] S. M. Lukyanov,[12] J. Mrázek,[13] F. Negoita,[3] F. de Oliveira,[1] Yu.-E. Penionzhkevich,[12] Zs. Podolyák,[14] M. G. Porquet,[15] F. Rotaru,[3] P. Roussel-Chomaz,[1] M. G. Saint-Laurent,[1] H. Savajols,[1] G. Sletten,[16] J. C. Thomas,[1] J. Timàr,[4] C. Timis,[3] and Zs. Vajta[4]

[1] *Grand Accélérateur National d'Ions Lourds (GANIL), CEA/DSM-CNRS/IN2P3, Caen, France*
[2] *Institut de Physique Nucléaire, IN2P3-CNRS, F-91406 Orsay Cedex, France*
[3] *Institute of Physics and Nuclear Engineering IFIN-HH, P.O. Box MG-6, 077125 Bucharest-Magurele, Romania*
[4] *Institute for Nuclear Research (MTA Atomki), P.O. Box 51, H-4001 Debrecen, Pf.51, Hungary*
[5] *National Superconducting Cyclotron Laboratory and Department of Physics and Astronomy, Michigan State University, East Lansing, MI 48824, USA*
[6] *TRIUMF, 4004 Wesbrook Mall, Vancouver, British Columbia, V6T 2A3 Canada*
[7] *Institut für Kernphysik, Technische Universität Darmstadt, 64289 Darmstadt, Germany*
[8] *ExtreMe Matter Institute EMMI, GSI Helmholtzzentrum für Schwerionenforschung GmbH, 64291 Darmstadt, Germany*
[9] *Université Bordeaux 1, CNRS/IN2P3, Centre d'Études Nucléaires de Bordeaux Gradignan, UMR 5797, Chemin du Solarium, BP. 120, 33175 Gradignan, France*
[10] *CEA, DAM, DIF, F-91297 Arpajon, France*
[11] *Royal Institute of Technology, Stockholm, Sweden*
[12] *FLNR, JINR, RU-141980 Dubna, Moscow region, Russia*
[13] *Nuclear Physics Institute, AS CR, CZ-25068 Rez, Czech Republic*
[14] *University of Surrey, GU2 7XH Guildford, United Kingdom*
[15] *CSNSM, CNRS/IN2P3 and Université Paris-Sud, Bât 104-108, F-91405 Orsay, France*
[16] *Niels Bohr Institute, University of Copenhagen, Denmark*

(Dated: January 6, 2015)

The structure of the ^{24}F nucleus has been studied at GANIL using the β decay of ^{24}O and the in-beam γ-ray spectroscopy from the fragmentation of projectile nuclei. Combining these complementary experimental techniques, the level scheme of ^{24}F has been constructed up to 3.6 MeV by means of particle-γ and particle-$\gamma\gamma$ coincidence relations. Experimental results are compared to shell-model calculations using the standard USDA and USDB interactions as well as ab-initio valence-space Hamiltonians calculated from the in-medium similarity renormalization group based on chiral two- and three-nucleon forces. Both methods reproduce the measured level spacings well, and this close agreement allows unidentified spins and parities to be consistently assigned.

PACS numbers: 21.60.Cs, 23.20.Lv, 27.40.+z

I. INTRODUCTION

Nuclear forces play a decisive role in our understanding of the structure of atomic nuclei, driving the creation and evolution of shell gaps, the onset of deformation, development of halo structures, and determining the limits of particle stability. The nuclear shell model provides a framework to determine the properties of nuclei from a set of single-particle energies (SPEs) and two-body matrix elements (TBMEs) defined in a given valence space outside some assumed inert core. When based only on two-nucleon (NN) forces within the valence space, the SPEs and TBMEs need suitable renormalization to experimental data to provide a precise description of nuclear structure. These "effective" SPEs and TBMEs implicitly capture the effects of many-body processes, such as core polarization, as well as neglected three-nucleon (3N) forces [1–4] and coupling to the particle continuum.

As the standard shell-model approach typically uses TBMEs that are independent of mass number A or simply scaled, it may become insufficient near the limits of stability, where the last nucleons are only loosely bound and have radial wavefunctions which extend to larger radii and couple to unbound states [5]. Reductions of the neutron-neutron TBME by 25% were required to model the structure of the neutron-rich C isotopes, which are a factor of two less bound than the O isotopes [6, 7]. More recently, the study of the weakly bound ^{26}F nucleus, which can be viewed as an ^{24}O core plus a deeply bound $d_{5/2}$ proton and an unbound $d_{3/2}$ neutron, has shown that a reduction of the $\pi d_{5/2} - \nu d_{3/2}$ TBME by about 20% better reproduced the energies of its $J = 1^+$, 2^+, 4^+ states [8]. In addition, recent theoretical calculations for states close to the neutron-separation threshold show that an increased role of coupling to the particle continuum may in part account for the modification of shell structure of dripline nuclei [9, 10].

The fluorine isotopic chain is well suited to study the evolution of valence-space interactions with increased valence neutron-to-proton asymmetry towards the dripline.

Moreover, many F isotopes are located near the doubly magic ^{16}O, ^{22}O and ^{24}O systems. Considering these O isotopes as almost inert cores, fluorine wavefunctions should then be weakly mixed, making possible the search for subtle effects related to their weak binding and proximity to the continuum. Located between ^{22}O and ^{24}O, ^{24}F is an excellent candidate for such a study, because its spectroscopy is expected to be relatively simple. As in ^{26}F, states located near the neutron separation energy, $S_n = 3.840(10)$ MeV, could be influenced by effects arising from asymmetric proton-to-neutron binding.

In a simple shell-model picture, the lowest-lying states in ^{24}F with spin-parity 2^+ and 3^+ can be considered pure $\pi d_{5/2} \otimes \nu s_{1/2}$ configurations on top of an ^{22}O core, while 0^+ and 1^+ states are expected from $\pi s_{1/2} \otimes \nu s_{1/2}$ configurations. Close to the dripline, the excitation of one neutron to the $d_{3/2}$ orbits gives rise to the $I^\pi = 1^+ - 4^+$ multiplet due to the $\pi d_{5/2} \otimes \nu d_{3/2}$ coupling observed at low energy in ^{26}F [8]. Configurations originating from neutron core excitations are also found below the neutron-separation threshold.

While previous β-decay studies [11, 12] agreed on the ^{24}O half-life (about 65 ms), deduced delayed-neutron emission probabilities differed significantly: P_n = 58(12)% in Ref. [11] and $P_n = 18(6)$% in Ref. [12]. From the latter work, it was expected that 82(6)% of the β strength would decay to bound states in ^{24}F [12]. Because only 60% of the β-decay strength was observed, it was proposed that this missing strength may feed higher-lying 1^+ excited state(s), likely of $\pi d_{5/2} \otimes \nu d_{3/2}$ origin, that could not be observed experimentally due to the lack of statistics. Three γ transitions associated with the decay of ^{24}O were observed [12], but the statistics were not sufficient to unambiguously establish a ^{24}F level scheme. No other spectroscopic information was known on ^{24}F before the present study.

To search for members of the $d_{5/2} - d_{3/2}$ multiplet, the spectroscopy of ^{24}F has been studied using two complementary experimental methods in this work. First, 1^+ states were accessed from the β decay of ^{24}O, which has an $I^\pi = 0^+$ ground state. In a separate experiment, higher-spin states were produced in the fragmentation of projectile nuclei leading to ^{24}F. The results were then compared to shell-model calculations based on the benchmark USDA and USDB empirical Hamiltonians [13] as well as ab initio valence-space Hamiltonians derived from NN+3N forces [14]. The excellent agreement between these two calculations results in a robust description of the newly measured states.

II. β-DECAY OF ^{24}O

A. Experimental set-up

The ^{24}O nucleus was produced via fragmentation of a $^{36}S^{16+}$ primary beam delivered by the GANIL facility in a 237 mg/cm^2 Be target placed at the entrance

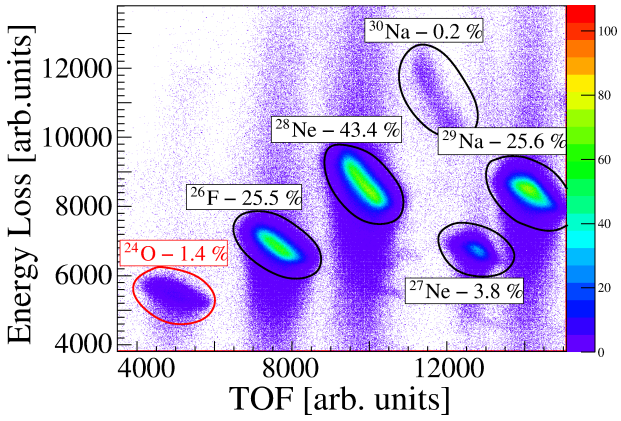

FIG. 1. (Color online) Energy loss versus time-of-flight identification matrix. The relative yields of the implanted ions are shown by different shades.

of the LISE spectrometer [15]. The energy and the average intensity of the primary beam were 77.6 MeV/u and 2 eμA, respectively. The projectile-like fragments were separated by the LISE achromatic spectrometer. A ^{9}Be wedge-shaped degrader of 1066 mg/cm^2 was placed at the dispersive focal plane of LISE to improve the ion selection. As shown in Fig. 1 the selected nuclei were identified at the end of the spectrometer by means of their energy loss (ΔE) in two silicon detectors of 500 μm thickness and their time-of-flight (TOF) referenced to the cyclotron radio-frequency. An Al foil of adjustable inclination was placed after the two Si detectors to allow the implantation depth of the ^{24}O ions into a 1 mm double-sided-silicon-strip detector (DSSSD) of 5×5 cm^2 with 16×16 strips. The pixels in the DSSSD were used to establish spatial and time correlations between the β-particles and the ^{24}O parent. Energy threshold of the individual strips were set to ∼80 keV. A 5 mm-thick Si detector was placed after the DSSSD to control the implantation depth of ^{24}O.

Four segmented Ge Clover detectors of the EXOGAM array [16] were placed around the DSSSD detector to provide $\beta - \gamma$ coincidences. A γ-ray efficiency ε_γ of 6.5% at 1 MeV was extracted from the β-decay of ^{28}Ne which was transmitted in the same set-up and for which the intensities of the γ transitions were known [17]. For each implanted nucleus, a β efficiency (ε_β) of 63(3)% was extracted from the intensity ratio between an identified γ-line gated or ungated on the β-correlation condition. The relative γ-ray intensities were obtained from the ε_β and ε_γ values.

B. Results

The β-gated γ-ray spectrum following the implantation of a precursor ^{24}O nucleus between 0–250 ms is shown in Fig. 2 a). This time condition favors the observation of γ rays associated to the decay of ^{24}F while it suppresses all

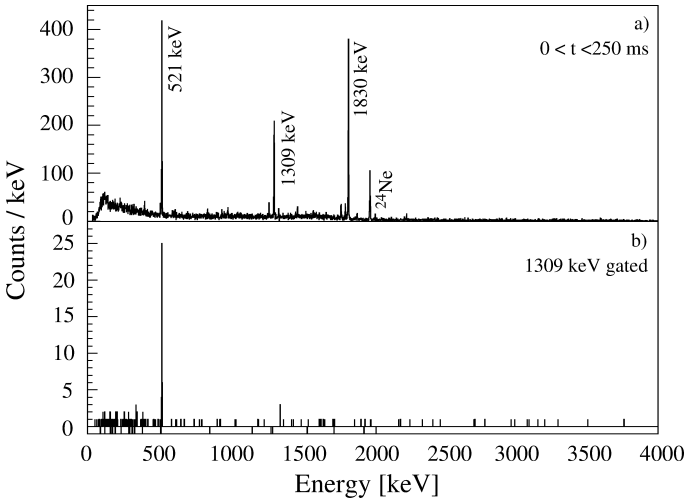

FIG. 2. a) β-gated γ-ray spectrum following the implantation of ^{24}O nuclei obtained in the 0–250 ms range. b) $\gamma\gamma$-coincidence spectrum gated by the 1309 keV γ-ray.

transitions belonging to contaminant nuclei or daughter activity. The previously reported γ-lines [12] at 521 keV, 1309 keV and 1830 keV are clearly visible. All other observed transitions are not attributed to the decay of ^{24}O.

A total of $\sim 10^5$ ^{24}O nuclei were implanted in the DSSSD detector, which is a factor of 10 larger than in Ref. [12]. The improved statistics obtained in the present work permitted a study of $\gamma\gamma$ coincidences (Fig. 2 b), from which it was deduced that the 1^+ level at 1830 keV is fed with I_β=57(4) % and decays by a cascade of 521 keV and 1309 keV γ-rays. The ordering of these two transitions could not be determined unambiguously from the β-decay study as they have the same relative intensity (Table I). The in-beam experiment presented in Section III B shows that the 1309 keV γ-ray feeds a level at 521 keV. The 1830 keV level decays by a competing branch directly to the ground state, as well. The γ-ray energies, relative intensities and branching ratios of the observed transitions are listed in Table I.

The background subtracted summed time-distribution of the 521 keV, 1309 keV and 1830 keV γ-rays with respect to the ^{24}O implantation is shown in Fig. 3. A fit with a single exponential decay-curve yields a half-life of $T_{1/2}$=80(5) ms, in agreement with the 61^{+32}_{-19} ms value of Ref. [11] within the statistical uncertainties but longer than the value of 65(5) ms reported in Ref. [12]. Using the β-decay Q-value and the absolute feeding intensity of the 1830 keV state a logft value of 4.25(6) has been obtained, which is consistent with an allowed Gamow-Teller transition.

The observational limit for the population of other 1^+ states has been measured to be 1.0(4)%. The β-delayed neutron emission probability has been extracted to be P_n=43(4)% from the yields of the 1830 keV and 1309 keV transitions normalized to the total number of ^{24}O detected. This value is in agreement with P_n = 58(12)% previously reported in Ref. [11] but larger than the value of 18(6)% measured in Ref. [12].

TABLE I. Experimental energies, spin and parity assignments, transition energies, relative intensities per 100 decays. γ branching ratio (BR) for the excited states of ^{24}F observed in the β-decay of ^{24}O experiment.

E_i [keV]	$I_i^\pi \rightarrow I_f^\pi$	E_γ [keV]	I_γ[\ 100 decays]	BR[%]
521(1)	$2_1^+ \rightarrow 3_1^+$	521(1)	21(2)	
1830(1)	$1_1^+ \rightarrow 3_1^+$	1830(1)	39(3)	68(5)
	$1_1^+ \rightarrow 2_1^+$	1309(1)	18(2)	32(3)

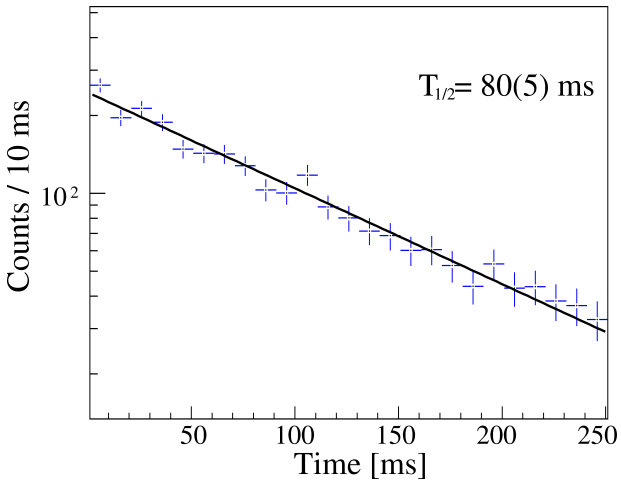

FIG. 3. (Color online) Background-subtracted summed time-distribution gated on the 521 keV, 1309 keV and 1830 keV γ-rays following the implantation of ^{24}O nuclei. The fit with a single exponential decay-curve yields $T_{1/2}$=80(5) ms.

In a separate setting of the LISE spectrometer, the β-decay of ^{24}F was studied as well. From this data set the direct feeding to the 2^+ state at 1981 keV and the 4^+ state at 3963 keV in ^{24}Ne were observed [18]. It establishes that the spin and parity of the ground state of ^{24}F is 3^+. It follows that the 521 keV state is located in between the 3^+ ground state and the 1^+ excited state at 1830 keV. As the 521 keV state is not populated directly in the ^{24}O β-decay its spin and parity must therefore be 2^+.

III. IN-BEAM SPECTROSCOPY OF THE ^{24}F NUCLEUS

A. Experimental set-up

The ^{24}F nucleus was produced in a two-step reaction. A ^{36}S primary beam of 77.5 A MeV with an average intensity of 6.5 eμA underwent fragmentation in a 398 mg/cm^2 C target placed between the two superconducting solenoids of the SISSI [19] device. The reaction products were separated and selected trough the ALPHA

spectrometer by means of the Bρ-ΔE-Bρ method [15, 20]. The transmitted cocktail beam was composed of ^{25,26}Ne, ^{27,28}Na and ^{29,30}Mg nuclei with energies ranging between 54 and 65 MeV/u. The identification of the beam ions was performed by the combined measurement of their time-of-flight (TOF) over a flight path of 80 m using two micro-channel plates and their energy loss in a plastic scintillator of 103.5 mg/cm^2 thickness located at the entrance of the SPEG spectrometer [21]. Two C foils of 51 mg/cm^2 thickness were placed before and after the plastic scintillator constituting a secondary "active" target. The ^{24}F nuclei were produced in this secondary target through the fragmentation of ^{27}Na. Once produced, the ^{24}F nuclei were separated from other reaction residues in the SPEG spectrometer. The identification of the ions was performed on an event-by-event basis at the final focal plane of the SPEG by measuring their time-of-flight (TOF) with a plastic scintillator, their energy loss (ΔE) and position in an ionization and two drift chambers, respectively. In addition, 74 BaF_2 detectors of the Château de Cristal array surrounded the secondary target at an average distance of 30 cm. Prompt γ-ray emission was measured in coincidence with the nuclei identified at the final focal plane of SPEG. The photopeak efficiency of the array was 24 %, 42 % and 29 % for γ-ray energies of 100 keV, 600 keV and 1300 keV, respectively.

B. Results

Prompt γ rays observed in coincidence with the ^{24}F nuclei identified in SPEG are listed in Table II. The singles γ-ray spectrum of ^{24}F is shown in Fig. 4. The three γ rays at 527(10) keV, 1309(22) keV and 1827(11) keV correspond, within the experimental uncertainties, to those observed in the β-decay of ^{24}O at 521(1) keV, 1309(1) keV and 1830(1) keV, respectively. The excitation energy of the 1829(26) keV state has been extracted by the weighted mean of the energies of the two decay branches. It is in agreement with the value obtained in the β-decay data set. The $\gamma\gamma$-coincidence between the 527 keV and 1309 keV transitions (Fig. 5 a) is confirmed. The ordering of the two transitions is obtained from their relative intensity since the 527 keV γ-ray intensity is much larger than that of the 1309 keV transition (Tab. II) the 527 keV state is placed below. It can be fed directly in the reaction and/or by other higher-lying excited states. In addition, four new transitions have been observed between 2200 keV and 4000 keV. To get a reasonable line shape, the response function of the BaF_2 array was simulated using the GEANT4 package. In the simulation the energy dependence of the peak width, the cut-off energy, the Doppler shift and the Doppler broadening were taken into account. The energy-dependent width of the γ ray peak has been extracted from the spectroscopy of other nuclei produced in similar experimental conditions [22]. For γ-rays with energies greater than ~1.5 MeV, in addition to the photo-absorption and

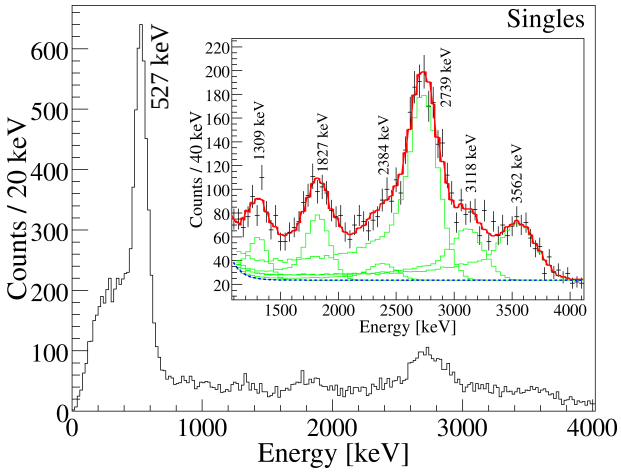

FIG. 4. (Color online) Singles γ-ray spectrum obtained in coincidence with the ^{24}F nuclei produced in the in-beam γ-ray spectroscopy experiment. The inset presents a zoom on the high-energy part of the spectrum. The lines show the result of the fit with line shapes obtained from GEANT simulation.

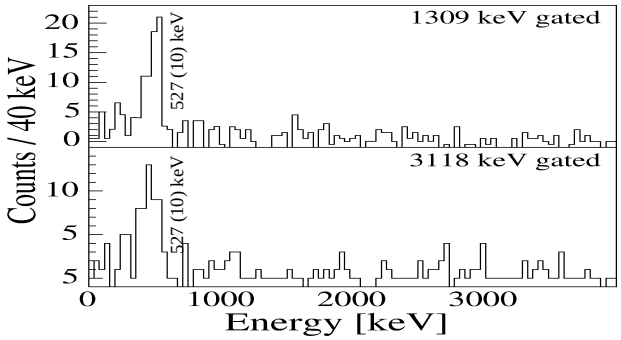

FIG. 5. $\gamma\gamma$ coincidence-spectra gated by the 1309 keV (a) and 3118 keV (b) transitions.

Compton effects pair creation also starts to play a significant role. Since an add-back procedure was used in the analysis of the γ-ray spectra, the escape of the annihilation and Compton scattered γ rays are suppressed. As a consequence, the line shape is well described using a Gaussian plus a long, low-energy tail. Using the simulated line shapes the γ-ray spectrum between 2.2 and 4.0 MeV could be described by four γ-rays at 2384(64), 2739(14), 3118(33) and 3562(22) keV (inset of Fig. 4).

A clear coincidence between the 527 keV and 3118 keV γ-rays is observed (Fig. 5 b)), establishing a state at 3639 keV excitation energy, considering that the 527 keV transition corresponds to the 521 keV γ-line observed in the β-decay experiment. No other $\gamma\gamma$-coincidences were observed, indicating that the 2384 keV, 2739 keV and 3562 keV transitions decay directly to the ground state. Therefore, three new excited states are proposed at 2384(64) keV, 2739(14) keV and 3562(22) keV.

TABLE II. Experimental energies, tentative spin and parity assignments, transition energies, relative feeding intensities and γ branching-ratios (BR) for the excited states in ^{24}F obtained in the in-beam spectroscopy experiment.

E_i [keV]	$I_i^\pi \rightarrow I_f^\pi$	E_γ [keV]	I_γ[%]	BR[%]
527(10)	$2_1^+ \rightarrow 3_1^+$	527(10)	71(3)	
1829(26)	$1_1^+ \rightarrow 3_1^+$	1827(11)	17(2)	77(10)
	$1_1^+ \rightarrow 2_1^+$	1309(22)	5(1)	23(5)
2384(64)	$(4_1^+) \rightarrow 3_1^+$	2384(64)	7(3)	
2739(14)	$(3_2^+) \rightarrow 3_1^+$	2739(14)	100(5)	
3562(22)	$(2_3^+, 4_2^+) \rightarrow 3_1^+$	3562(22)	47(5)	
3639(42)	$(1_2^+, 2_2^+) \rightarrow 2_1^+$	3118(33)	34(3)	

IV. DISCUSSION

The experimental level scheme deduced in the discussed experiments up to the neutron separation energy of 3.84 MeV is shown in Fig. 6. The spin and parity of the previously reported 1830 keV state [12] can be firmly established to be 1^+ from the β-decay of ^{24}O. The level scheme has been completed by four new states at higher excitation energy. In order to clarify their spin and parity assignment, the experimental excitation energies and branching ratios were compared to predictions of different theoretical calculations (Fig. 6).

The shell-model calculations were performed using the standard USDA and USDB interactions [13, 24] in the full *sd* valence space. The data used in the USDA/USDB fit comprises ground states and low-lying excited states of the *sd*-shell nuclei from A = 16 to A = 40, therefore the experimental binding energy of the ground state of ^{24}F is in agreement with the theoretical predictions.

In order to assign the spins of the observed states, the experimental branching ratios were compared to the theoretical ones extracted from the E2 to M1 decay branch of each state, re-scaled in energy to match the experimental value. Starting from spin assignments of the low-energy levels, the higher-energy ones can be deduced. In the calculation of the M1 reduced transition probabilities, the effective g-factors of the proton (neutron) $g_{sp} = 5.0$ (g_{sn} = -3.44), $g_{lp} = 1.174$ (g_{sn} = -0.110) and $g_{tp} = 0.24$ (g_{tn} = -0.16) for the spin, orbital and tensor components of the M1 operator are taken from Ref. [24]. The E2 reduced transition probabilities are calculated using effective charges of 1.36e and 0.45e for protons and neutrons, respectively.

The spin and parity assignment of the experimental state at 527 keV is 2_1^+. The USDA interaction underestimates the excitation energy by ∼200 keV while better agreement is found in the USDB calculations. This 2_1^+ level decays 100% to the 3^+ ground state of ^{24}F. Both levels belong to the $\pi d_{5/2} \otimes \nu s_{1/2}$ multiplet with an almost pure wave function (∼70%).

The excitation energy of the 1_1^+ state at 1830 keV, which originates mainly (∼50%) from a mixed $\pi s_{1/2} \otimes \nu s_{1/2}$ configuration, is underestimated in the USDA and USDB calculations. A somehow similar shift in energy between experiment and theory is found for the $1/2^+$ state in ^{25}F [23], that is due to an $s_{1/2}$ proton excitation. The 1_1^+ level decays by a 1830 keV transition to the ground state (77(10)%) and by a parallel branch to the 521 keV level (23(5)%), which agrees with the USDB calculations of 72% and 28%, respectively. The USDA calculations result in 95% decay to the ground state and 5% to the 2_1^+ level. The reduced M1 matrix element is 0.11 μ_N with USDA and 0.17 μ_N with USDB. This difference is consistent with the results shown in Figure 2 of Ref. [24] where M1 matrix elements for USDA and USDB differ in a random way with a root-mean square (r.m.s.) difference of about 0.10 μ_N being about the same for large and small values. As suggested in [24], the r.m.s. difference between experimental and theoretical M1 matrix elements might be reduced if some of the M1 data could be used to constrain the Hamiltonian.

The level at 2384 keV decays exclusively to the ground state. The only theoretical counterpart having the same decay pattern is the 4_1^+ state, which has a 73% pure $\pi d_{5/2} \otimes \nu (d_{5/2})^{-1} (s_{1/2})^2$ configuration.

The energy spacing of the experimental levels between 2400 keV and 3700 keV is better reproduced in the calculations performed with the USDA interaction. The results obtained with the USDB interaction show a spectrum with states having a regular spacing. Both calculations predict a high density of levels at high excitation energy close to the neutron separation energy, among them the 1_2^+ and 4_2^+ states belonging to the $\pi d_{5/2} \otimes \nu d_{3/2}$ multiplet. These levels are of the same origin as the 1_1^+ and 4_1^+ states in the low-energy spectrum of the weakly bound ^{26}F nucleus.

The spin and parity of the 2739 keV state is tentatively assigned to be 3_2^+ because any other possibility would imply a deviation between the experimental and theoretical excitation energy of more than 400 keV. Experimentally, this state decays by more than 95% to the 3_1^+ ground state in contrast to the calculations that give 3, 84, 12 % to the 3_1^+, 2_1^+, 4_1^+ states for USDA, respectively, and 15, 38, 47 % for USDB. The difference between experiment and theory might come from the fact that the B(M1) value to the ground state is very small: 0.0010 μ_N^2 for USDA and 0.0017 μ_N^2 for USDB. A B(M1) value of 0.010 μ_N^2 would give 90 % branch to the ground state. The corresponding M1 matrix elements are 0.083 μ_N (USDA) and 0.110 μ_N (USDB) and 0.26 μ_N for B(M1)=0.010 μ_N^2. This range of matrix elements is within the overall best-fit r.m.s. deviation between experimental and theoretical M1 matrix elements of 0.20 μ_N (Table I in [24]). The 3_2^+ level belongs to the same multiplet as the 4_1^+ state with a ∼53% pure configuration.

At higher excitation energies there is a large density of calculated levels which make the spin and parity assignments to the experimental 3562 keV and 3639 keV states difficult. The experimental branching ratios were compared to the calculated decay pattern of the 4_2^+, 2_3^+, 2_2^+ and 1_2^+ levels. The I^π of the 3562 keV level is tentatively

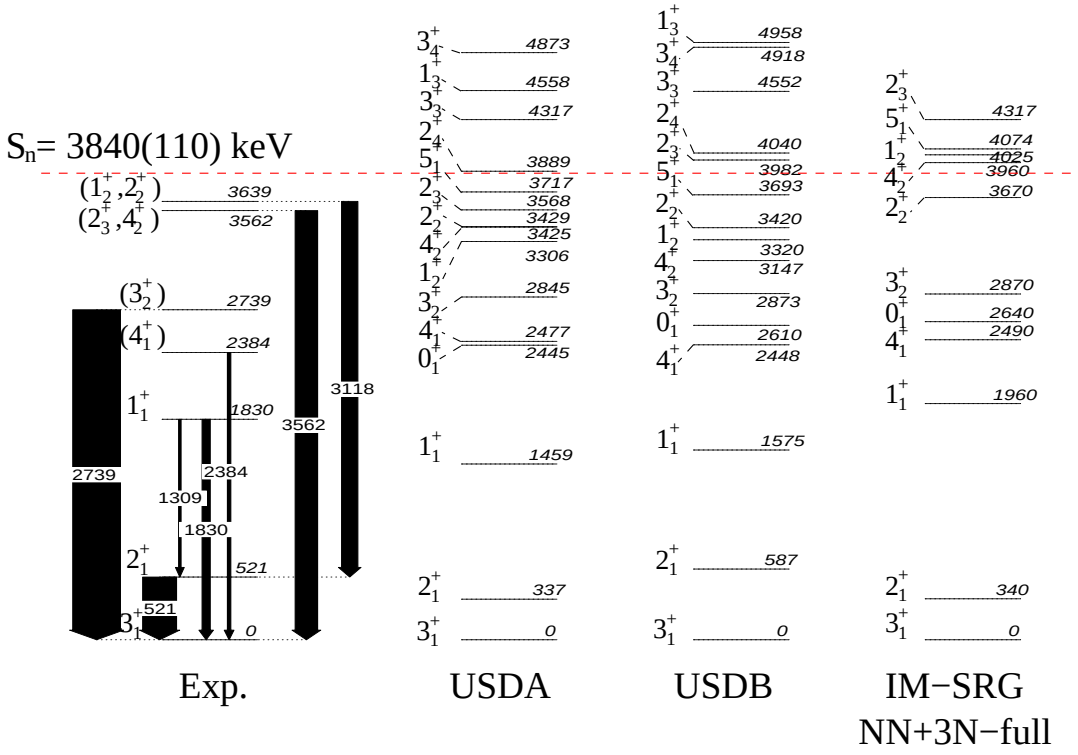

FIG. 6. (Color on line) Experimental level scheme of ^{24}F obtained in the in-beam and β-decay data set compared to shell-model calculations performed with the USDA and USDB interactions as well as ab-initio valence-space Hamiltonians calculated from the in-medium similarity renormalization group.

assigned to be 4_2^+ or 2_3^+, that of the 3639 keV state 2_2^+ or 1_2^+. The 3562 keV state is a good candidate for the 4_2^+ which belongs to the $\pi d_{5/2} \otimes \nu d_{3/2}$ multiplet with ∼64% pure configuration. It would be favorably populated in the reaction due to being an Yrast state. As no evidence of the existence of a 1_2^+ state was found in the β-decay experiment, the 3639 keV state is likely to be I = 2_2^+. The 2_2^+ and 2_3^+ levels have very mixed and complex wave functions.

In addition, theoretical predictions from first-principles valence-space calculations, where the many-body processes and 3N forces are included are explored. Effective shell-model Hamiltonians based on two-nucleon (NN) and 3N forces were first derived for the sd-shell region within the context of many-body perturbation theory [3, 26–29], where excitations outside the valence space were calculated to third order. There it was found that both 3N forces as well as an extended valence space (i.e., including orbitals beyond the standard sd shell), were essential to describe semi-magic isotopic/isotonic chains on top of a ^{16}O core. The need for an extended space in the perturbative calculation of the valence-space Hamiltonian suggests that the extended orbitals need to be included nonperturbatively.

Therefore, it has been considered in this paper a novel nonperturbative method for constructing valence-space Hamiltonians: the in-medium similarity renormalization group (IM-SRG) [14, 30–32]. In addition to the IM-SRG other ab initio methods have now successfully treated the oxygen chain and select fluorine and neon isotopes with NN+3N forces [33–36]. In the IM-SRG, a continuous unitary transformation, parameterized by the flow parameter s, is applied to the initial normal-ordered A-body Hamiltonian such that undesirable off-diagonal couplings are driven to zero as $s \to \infty$:

$$H(s) = U^\dagger(s) H U(s) = H^{\rm d}(s) + H^{\rm od}(s)\,, \qquad (1)$$

$$H^{\rm od}(s \to \infty) = 0\,. \qquad (2)$$

Taking the uncorrelated ground state of doubly magic ^{16}O, and defining $H^{\rm od}$ to be all n-particle-n-hole excitations, $H(s \to \infty)$ will flow to the fully correlated (i.e., exact) ground-state energy as $H^{\rm od}(s) \to 0$. Including excitations that connect valence-space to non-valence-space particle states in the definition of $H^{\rm od}$, the *sd* valence space will decouple from the core and higher shells as $s \to \infty$. The resulting Hamiltonian $H(\infty)$ will then consist of renormalized *sd*-shell SPEs and TBMEs, to be used as input in a standard shell-model calculation, in addition to the ^{16}O core energy [14, 31].

The starting point for these calculations are nuclear forces derived from chiral effective field theory [37, 38]. We use the 500 MeV-cutoff N^{3}LO NN potential of Ref. [39] and the local N^{2}LO 400 MeV-cutoff 3N interaction of Ref. [40], evolved with the free-space SRG

[41] to a lower momentum scale, $\lambda_{\rm SRG} = 1.88\,{\rm fm}^{-1}$. IM-SRG *sd*-shell Hamiltonians are then calculated following the procedure outlined above, based on SRG-evolved NN forces with 3N forces induced by the SRG evolution (NN+3N-induced) as well as with initial 3N forces (NN+3N-full). The latter are included through normal ordering with respect to the ^{16}O Hartree-Fock reference state, truncated at the two-body level [42, 43]. For complete details, see Ref. [14]. Finally, the resulting shell-model Hamiltonians are diagonalized to obtain the spectrum of ^{24}F, studying for the first time IM-SRG proton-neutron valence interactions.

Without initial 3N forces, the spectrum (not shown) is much too compressed and the ordering of levels is incorrect: The first eight excited states lie below 2.0 MeV, in clear contrast to experiment and the NN+3N-full results shown in Fig. 6. While the ground-state energy of ^{24}F is overbound by 7.7 MeV in the NN+3N-full calculation, the predicted excited-state spectrum is in remarkably good agreement with the new experimental measurements. In particular, all excited states below the one-neutron separation threshold are less than 200 keV away from corresponding experimental levels. The only exception is a 0_1^+ state at 2640 keV, also predicted with USDA,B, which is likely not seen experimentally due to the difficulty of the fragmentation method in populating low-J states. Since coupling to the continuum is currently neglected, when included, a modest lowering of the 2_2^+, 4_2^+, 1_1^+, and 5_1^+ states would be expected near threshold. Furthermore the wavefunctions and γ transitions involving these states are very similar to those discussed above for USDA,B, strengthening the proposed identifications made for the 3_2^+ and 4_1^+ states. Specifically the $3_2^+ \rightarrow 3_1^+$ branch is 26%, in moderately better agreement with experiment. The probable identification of the 3639 keV level as the 2_2^+ state suggests an incorrect $2_2^+ - 4_2^+$ ordering is seen in these calculations. This can be understood in terms of neglected continuum effects: The $\nu{\rm d}_{3/2}$ component of the 4_2^+ state is twice as large as that in 2_2^+, hence one would naively expect that, when added, the continuum would then lower the 4_2^+ by a greater amount than the 2_2^+, possibly resulting in the correct ordering. This hypothesis needs to be confirmed by an unambiguous location of the 2_2^+ and 4_2^+ states in ^{24}F and more detailed theoretical calculations. Recent coupled-cluster calculations based on optimized N^{2}LO chiral NN and 3N forces have been performed for ^{24}F [36], which exhibit reasonable agreement with this new experimental picture.

V. SUMMARY

Detailed spectroscopy of the ^{24}F nucleus has been obtained at GANIL using two complementary experimental techniques: β decay and in-beam γ-ray spectroscopy from projectile fragmentation. Previously reported transitions (521, 1309 and 1830 keV) have been confirmed, and in addition four new γ rays have been observed for the first time. The γ-ray ordering was established from relative intensity arguments and the large statistics of the present data allowed to perform a $\gamma\gamma$-coincidences analysis. Gathering all the available information on ^{24}F, a level scheme has been proposed up to the neutron separation energy. The ground state spin and parity of ^{24}F is unambiguously determined to be 3^+. Excitation energies and branching ratios are compared to two shell-model calculations (using the standard USDA and USDB interactions) as well as to ab initio shell-model calculations, using interactions derived from chiral NN+3N forces by means of the IM-SRG. From this comparison a clear identification of almost all measured states has been obtained. It is suggested that the 3_1^+ ground state and the 2_1^+ levels belong to the $\pi{\rm d}_{5/2} \otimes \nu{\rm s}_{1/2}$ multiplet with more than 70% pure wavefunctions. The 1_1^+ state has a predominant $\pi{\rm s}_{1/2} \otimes \nu{\rm s}_{1/2}$ configuration, while the 4_1^+ and 3_2^+ states have predominant $\pi{\rm d}_{5/2} \otimes \nu({\rm d}_{5/2})^{-1}({\rm s}_{1/2})^2$ configurations. At higher excitation energy, the large density of observed and calculated states makes the identification of the experimental levels more ambiguous. Tentative 2_2^+ and 4_2^+ spin parity values are proposed for the 3639 keV and 3562 keV levels, respectively. Their ordering is only reproduced by the shell model using the USDA and USDB interactions, while the calculations performed with the IM-SRG predicts an inversion of the two states. As being significantly less mixed than the 2_2^+ state, the 4_2^+ is expected to be more sensitive to continuum effects, and therefore the explicit treatment of such effects should lower its energy by a greater amount than the 2_2^+. This would possibly result in the correct ordering in the IM-SRG model. Further spectroscopic information of ^{24}F at high excitation energy and more detailed theoretical calculations will be needed to elucidate the role of the continuum in the high-energy part of the level scheme of this nucleus, but the overall agreement between IM-SRG theory and experiment is globally extremely satisfactory.

ACKNOWLEDGMENTS

The authors are thankful to the GANIL and LPC staffs and the EXOGAM collaboration. This work has been supported by the European Community contract no. RII3-CT-2004-506065, by OTKA K100835 and NN104543, by the NSF PHY-1068217 grants, by a grant of the Romanian National Authority for Scientific Research, CNCS - UEFISCDI, project no. PN-II-ID-PCE-2011-3-0487. We thank S. Binder, A. Calci, J. Langhammer, and R. Roth for providing us with chiral 3N matrix elements. Computing resources for the IM-SRG calculations were provided by the Ohio Supercomputer Center (OSC).

[1] E. Caurier *et al.*, Rev. of Mod. Phys. **77**, 427 (2005).
[2] M. Hjorth-Jensen, T. T. S. Kuo and E. Osnes, Phys. Rept. **261**, 125 (1995).
[3] T. Otsuka *et al.*, Phys. Rev. Lett. **105**, 032501 (2010).
[4] J. D. Holt, T. Otsuka, A. Schwenk and T. Suzuki, J. Phys. G **39**, 085111 (2012).
[5] J. Dobaczewski *et al.*, Prog. Part. Nucl. Phys. **59**, 432 (2007).
[6] M. Stanoiu *et al.*, Phys. Rev. C **78**, 034315 (2008).
[7] C. M. Campbell *et al.*, Phys. Rev. Lett. **97**, 112501 (2006).
[8] A. Lepailleur *et al.*, Phys. Rev. Lett. **110**, 082502 (2013).
[9] I. Hamamoto, Phys. Rev. C **85**, 064329 (2012).
[10] G. Hagen *et al.*, Phys. Rev. Lett. **109**, 032502 (2012).
[11] A. C. Mueller *et al.*, Nucl. Phys. A **513**, 1 (1990).
[12] A. T. Reed *et al.*, Phys. Rev. C **60**, 024311 (1999).
[13] B. A. Brown and W. A. Richter, Phys. Rev. C **74**, 034315 (2006).
[14] S. K. Bogner *et al.*, Phys. Rev. Lett. **113**, 142501 (2014).
[15] R. Anne *et al.*, Nucl. Instr. Methods A **257**, 215 (1987).
[16] J. Simpson *et al.*, Acta Physica Hungarica, New Series, Heavy Ion Physics **11**, 159 (2000).
[17] V. Tripathi *et al.*, Priv. Communications (2011).
[18] A. Lepailleur, PhD Thesis, Université de Caen Basse Normandie, https://tel.archives-ouvertes.fr/tel-01057890/document
[19] E. Baron, J. Gillet and M. Ozille, Nucl. Instr. Methods A **362**, 90 (1995).
[20] J. P. Dufour *et al.*, Nucl. Instr. Methods A **248**, 267 (1986).
[21] L. Bianchi *et al.*, Nucl. Instr. Methods A **276**, 509 (1999).
[22] M. Stanoiu, PhD thesis, Université de Caen (2002).
[23] Z. Vajta et al., Physical Review C **89**, 054323 (2014).
[24] W. A. Richter, S. Mkhize and B. A. Brown, Phys. Rev. C **78**, 064302 (2008).
[25] B. A. Brown, Phys. Rev. C **58**, 220 (1998).
[26] J. D. Holt, J. Menéndez and A. Schwenk, Eur. Phys. J. A **49**, 39 (2013).
[27] J. D. Holt, J. Menéndez and A. Schwenk, Phys. Rev. Lett. **110**, 022502 (2013).
[28] C. Caesar *et al.* (R3B/LAND collaboration), Phys. Rev. C **88**, 034313 (2013).
[29] A. T. Gallant *et al.*, Phys. Rev. Lett **113**, 082501 (2014).
[30] K. Tsukiyama, S. K. Bogner and A. Schwenk, Phys. Rev. Lett. **106**, 222502 (2011).
[31] K. Tsukiyama, S. K. Bogner and A. Schwenk, Phys. Rev. C **85**, 061304(R) (2012).
[32] H. Hergert *et al.*, Phys. Rev. C **87**, 034307 (2013).
[33] G. Hagen, M. Hjorth-Jensen, G. R. Jansen, R. Machleidt, and T. Papenbrock, Phys. Rev. Lett. **108**, 242501 (2012).
[34] H. Hergert, S. Binder, A. Calci, J. Langhammer and R. Roth, Phys. Rev. Lett. **110**, 242501 (2013).
[35] A. Cipollone, C. Barbieri and P. Navrátil, Phys. Rev. Lett. **111**, 062501 (2013).
[36] A. Ekström et al., arXiv:1406.4696
[37] E. Epelbaum, H.-W. Hammer and U.-G. Meißner, Rev. Mod. Phys. **81**, 1773 (2009).
[38] R. Machleidt and D. R. Entem, Phys. Rep. **503**, 1 (2011).
[39] D. R. Entem and R. Machleidt, Phys. Rev. C **68**, 041001 (2003).
[40] R. Roth, S. Binder, K. Vobig, A. Calci, J. Langhammer and P. Navrátil, Phys. Rev. Lett. **109**, 052501 (2012).
[41] S. K. Bogner, R. J. Furnstahl and R. J. Perry, Phys. Rev. C **75**, 061001(R) (2007).
[42] G. Hagen *et al.*, Phys. Rev. C **76**, 034302 (2007).
[43] R. Roth *et al.*, Phys. Rev. Lett. **109**, 052501 (2012).